*Indonesian Journal of Aerospace Vol. 32 No. 2 December 2025 : pp 95–116 (Fahrizal et al.)*
DOI: 10.55981/ijoa.2025.8981
https://ejournal.brin.go.id/ijoa/

# Implementation of Kalman Filter for Accuracy Improvement and Angular Stability as a Control Reference Parallel Manipulator for Camera Pointing on CAN Satellite

**Muhammad Fahrizal[1], Nofria Hanafi[1]**

[1]Department of Mechanics and Energy, Politeknik Elektronika Negeri Surabaya, Indonesia
e-mail: fahrizal@me.student.pens.ac.id, hanafi@pens.ac.id

Received: 10-12-2024. Accepted: 21-04-2025. Published: 12-02-2026

**Abstract**

This study focuses on the application of the Kalman Filter to improve the accuracy and stability of angular data obtained from Inertial Measurement Unit sensors, which are often affected by noise and bias. The refined angular data serves as a control reference for the parallel manipulator used in the camera pointing system on CAN satellites. Accurate and stable reading angles are essential to ensure precise camera alignment, especially in dynamic environments with disturbances. This study integrates the Kalman Filter into the IMU data processing pipeline to filter the raw roll, pitch, and yaw. We tested the yaw stability improvement by 5.29% and filter performance improvement with 29.25% accuracy, pitch stability improved by 4.63% with 31.12% filter accuracy improvement, and roll stability improved by 1.71% with 28.99% filter accuracy improvement. These filtered angles are then used to control the parallel manipulator, allowing for precise orientation adjustment. The system performance is evaluated in terms of angular accuracy, stability, and manipulator responsibility. The results show a significant improvement in the angular quality of the data, with reduced noise and bias, leading to improved manipulator control. This implementation supports the development of high-precision camera systems for CAN satellites, which require robust and reliable orientation mechanisms. The proposed approach contributes to advancing control systems in small-scale satellite technology, where accuracy and stability are of critical importance. This study highlights the potential of the Kalman Filter in enhancing sensor accuracy for CAN satellite camera pointing systems. However, further research is needed to address dynamic environmental variations that may affect sensor performance. Future studies could explore integrating complementary filtering techniques or machine learning models to optimize data fusion and improve overall system resilience.

***Keywords***: Kalman Filter; Parallel manipulator, CanSat, Inertial Measurement Unit

## Nomenclature (Optional)

| | | |
|---|---|---|
| $\hat{x}_{k\|k-1}$ | = | Prediction from time t to t-1 |
| $u_k$ | = | Control input time |
| $P_{k\|k-1}$ | = | Prediction error covariance |
| $Q$ | = | Noise covariance |
| $K_k$ | = | Kalman gain |
| H | = | Measurement matrix |
| $R$ | = | Measurement noise covariance |
| $z_k$ | = | Actual measurement of time |
| $I$ | = | Identity matrix |
| θ | = | Roll, ° |
| φ | = | Pitch, ° |
| ψ | = | Yaw, ° |

## 1. Introduction

In recent years, CubeSat and small satellite technologies have gained significant attention due to their cost-efficiency, rapid development cycles, and diverse applications, such as Earth observation, communication, and scientific experiments(Asundi & Fitz-Coy, 2013). Among these small satellites, CAN satellites stand out for their compact design and mission versatility. One critical challenge in their operation is achieving precise camera pointing for imaging and data acquisition tasks. Accurate orientation of the camera system is essential to ensure high-quality data, particularly when operating in dynamic and disturbance-prone environments such as low Earth orbit (LEO).

The pointing system of a satellite camera typically relies on angular data obtained from Inertial Measurement Unit (IMU) sensors, which measure roll, pitch, and yaw. However, raw data from IMU sensors often contain significant noise and bias, which can adversely affect the performance of control systems. These inaccuracies necessitate robust filtering techniques to enhance data reliability. The Kalman Filter is a widely recognized algorithm for filtering and estimating sensor data, offering real-time capabilities and the ability to minimize noise while accounting for sensor biases(Narasimhappa et al., 2020). While the Kalman Filter is a widely adopted solution for sensor data filtering, alternative methods such as the Particle Filter and the Complementary Filter have also been investigated for similar applications (Li & Wang, 2013). These methods offer varying degrees of accuracy and computational efficiency, which may present viable solutions for different operational scenarios. A broader exploration of these techniques could provide comparative insights into their suitability for CAN satellite applications.

This research aims to implement a Kalman Filter to improve the accuracy and stability of IMU angular measurements. The filtered data will be used as control references for a parallel manipulator tasked with precise camera orientation. Parallel manipulators are known for their structural rigidity, high accuracy, and ability to handle complex motion trajectories, making them an ideal choice for this application(Fadaei et al., 2019).

This paper details the integration of the Kalman Filter into the IMU data processing pipeline and its application to a parallel manipulator for camera pointing on a CAN satellite. The system's performance is evaluated based on its ability to reduce angular measurement noise, maintain stability, and ensure accurate pointing under various operational scenarios. This work contributes to the advancement of high-precision control systems for small-scale satellite technology, addressing key challenges in maintaining reliable and stable camera pointing mechanisms.

## 2. Methodology

This section entailed objectives of improving angular data accuracy and stability for controlling a parallel manipulator in a CAN satellite's camera pointing system. A structured methodology is proposed, focusing on data acquisition, filtering, system integration, testing, and evaluation. This methodology ensures a systematic approach to addressing the challenges posed by noisy and biased IMU data and their impact on the manipulator's performance. To validate the efficacy of the Kalman Filter, statistical analysis, including Mean Absolute Error (MAE) and Root Mean Square Error (RMSE), was conducted. Additionally, comparative testing with a Moving Average Filter was performed to highlight the advantages of the Kalman Filter in dynamic conditions. This comparative analysis underscores the robustness of the Kalman Filter in reducing noise and stabilizing sensor output

### 2.1. System Design and Architecture

### 2.1.1 Canned Satellite

CanSat (Cans-Satellite) is a small satellite model that is shaped like a CAN but has sensors and telemetry. The purpose of making CanSat is to teach how to build satellites on a small scale (Ramadhan et al., n.d.). The CanSat concept was created to be a cheap and simple solution for students to learn the basics of designing, developing, launching and operating satellites. The CAN Satellite model used for the prototype is shown in (Figure 2-1). It can show that the design of the vehicle is in the form of a cylinder with certain dimensions to accommodate the regulations of a launch mission.

**Figure 2-1:** Canned Satellite.

Commonly, CanSat is launched using a rocket or balloon up to hundreds of meters, then when in the air, CanSat performs several tasks, such as collecting sensor data, such as air pressure data, temperature, orientation, and location. Then the data is transmitted to the receiver on Earth via a specific communication protocol. After the mission in the air is complete, CanSat will descend using a parachute at a certain speed, so that when it hits the ground, there is no serious damage. For some missions, CanSat is required to have an additional landing gear mechanism during the landing process.

### 2.1.2 On-Board Data Handling

OBDH (On-Board Data Handling) has the main task of performing various tasks, such as sensor data acquisition, including temperature and accelerometer. On the other hand, OBDH also has other tasks, such as data storage and data transmission to the ground control station(Urandra et al., 2016). In an On-Board Data Handling, there is a main processor that will be the center of the system or the core of a satellite system. Its tasks are very complex and are responsible for the running of a space mission. Therefore, a chip with the right specifications is needed to run a space mission. Primarily, it can run satellite functionality and be able to survive in extreme conditions during launch to orbit in the atmosphere.

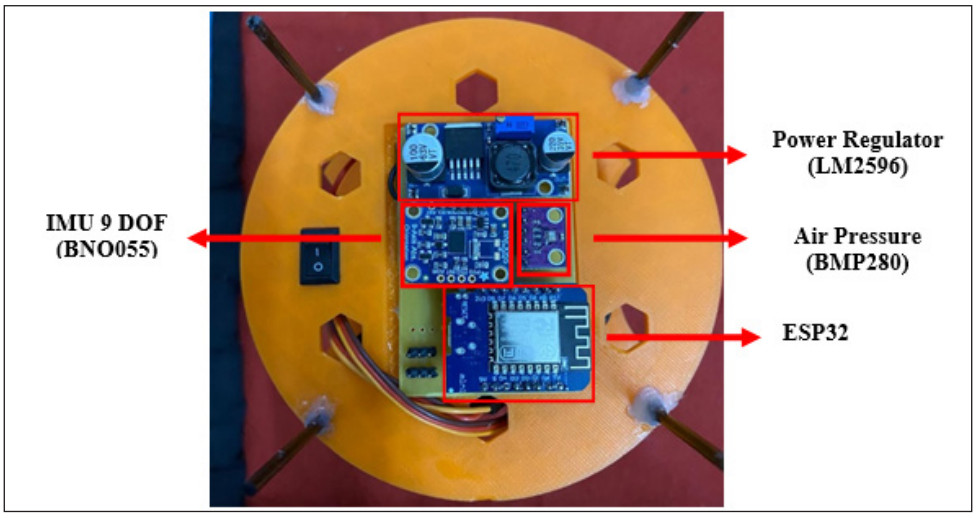


**Figure 2-2:** On-Board Data Handling.

There are many considerations when choosing a processor for a satellite vehicle, such as a Cansat. Considerations that must be understood as a satellite vehicle developer are the computing process with a high clock speed frequency, which will be very useful when OBDH performs quite complex tasks. Such as (Figure 2-2) is on-board data handling powered by the ESP8266 processor. With this, all tasks on the satellite mission can be quickly and precisely, so that the data received and processed becomes real-time. Then the standardization of processor manufacturing, which must be certified to withstand vibrations, extreme temperatures, and be able to withstand high air pressure.

### 2.1.3 Sensor IMU (*Inertial Measurement Unit*)

BNO055 is an advanced Inertial Measurement Unit (IMU) sensor developed by Bosch Sensortech. This sensor is known for its high integration, combining multiple sensors in one package, and its ability to provide orientation data directly (Farahan et al., 2022). This sensor consists of a 3-axis Gyroscope, 3-axis Accelerometer, and 3-axis Magnetometer, so it can be called 9 degrees of freedom (DOF). It can be shown in (Figure 2-3).

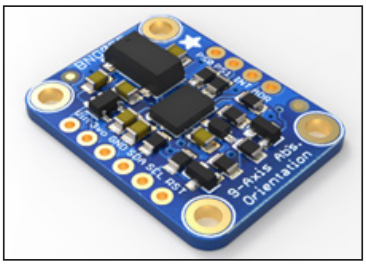

**Figure 2-3:** 9 DOF Inertia Measurement Unit.

This sensor has the ability to combine all data obtained by the sensor to be processed into accurate data, commonly called the fusion algorithm. This sensor is capable of producing a quaternion, as well as Euler angles (roll, pitch, and yaw), linear acceleration, and the gravity vector. On CanSat, BNO055 can function as the CanSat motion parameters displayed on the GCS (Ground Control Station).

### 2.1.4 Parallel Manipulator

A Parallel Manipulator is a robotic mechanism that allows a moving platform to be oriented in two degrees of rotational freedom, namely rotation around two mutually perpendicular axes. This manipulator has a parallel design characteristic, meaning the platform is moved by two or more arms that work simultaneously and are connected to actuators at its base (Palmieri et al., 2014). applications in several fields such as medical, aerospace, and robotics because the purpose of its formation is agility when operating and accuracy in angular reach.

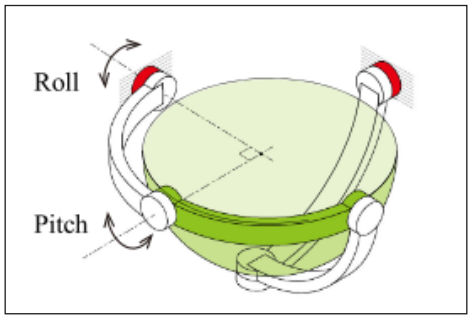


**Figure 2-4:** Spherical Parallel Manipulator (SPM).

2-DOF Parallel Manipulator is a robotic mechanism driven by two servo motors, each controlling one degree of freedom on a moving platform seen in (Figure 2-4) is a model of a 2 doff parallel manipulator. The first servo motor is responsible for controlling the rotation angle of the first arm, while the second servo motor controls the rotation angle of the second arm. Each arm is connected to the moving platform via revolute joints, so that when the two servo motors operate, they together produce rotational motion of the platform around two principal axes x on Eq. 2-1, and axes y on Eq. 2-2. The equation below is Forward Kinematics.

Equation Axes Roll (θθ):

$$Rx(\theta) = \begin{pmatrix} 1 & 0 & 0 \\ 0 & \cos(\theta) & -\sin(\theta) \\ 0 & \sin(\theta) & \cos(\theta) \end{pmatrix} \qquad (2-1)$$

$$Ry(\varphi) = \begin{pmatrix} \cos(\varphi) & 0 & \sin(\varphi) \\ 0 & 1 & 0 \\ -\sin(\varphi) & 0 & \cos(\varphi) \end{pmatrix} \qquad (2-2)$$

In inverse kinematics, the rotation matrix is known, Eq. 2-3, and we find the angle of each motor in the manipulator.

$$Mrot = \begin{pmatrix} r11 & r12 & r13 \\ r21 & r22 & r23 \\ r31 & r32 & r33 \end{pmatrix} \qquad (2-3)$$

$$\theta = arcsin(r32) \qquad (2-4)$$

$$\varphi = arctan(-r12, r22) \qquad (2-5)$$

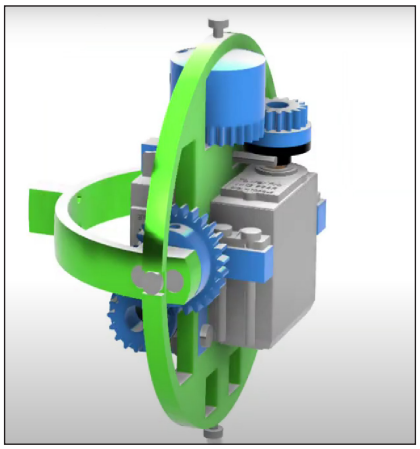

**Figure 2-5:** CAD design SPM 2 DOF.

The moving platform is designed to be oriented according to the change in rotation angle generated by the servo motor. This orientation setting allows the platform to direct the object mounted on it to various angular positions with high precision. The control signal is sent to the servo motor in the form of PWM (Pulse Width Modulation) pulses, which determine the rotation angle of each servo. With the angular coordination between the two servos, the manipulator is able to produce flexible and accurate platform orientation within a given workspace. The design of the manipulator model can be seen in (Figure 2-5).

The use of servo motors as actuators provides the advantages of fast response, precise control, and easy integration into robotic systems. The combination of two-arm mechanisms, rotary joints, and servo motors makes the 2-DOF Parallel Manipulator ideal for applications requiring precise and stable platform orientation.

### 2.2. Angular Estimation

Euler angles are a way to represent the orientation of an object in three-dimensional space using three rotation angles: roll, pitch, and yaw. These angles describe how an object changes position relative to a fixed reference frame, with rotations performed sequentially around three principal axes: x,y, and z.

Roll is the angle of rotation around the $x$ axis, which describes how the object tilts to the left or right. This rotation is often used to indicate rolling motion, such as an airplane or vehicle performing a turning maneuver. Pitch, on the other hand, is the angle of rotation around the y-axis, which indicates tilting up or down. This angle represents how the front of an object, such as an airplane or camera, moves up or down in three-dimensional space. Finally, yaw is the angle of rotation around the z-axis, which indicates the shift in direction or orientation of the object relative to the horizontal, such as the turning motion of a compass.

These three angles are calculated based on the rotation matrix, which is a mathematical representation of the orientation of the object (Kadir et al., 2020). The rotation matrix allows the transformation from the coordinates of the reference frame to the object frame, so that the orientation can be decomposed into Euler angles. To calculate the roll, pitch, and yaw angles from the rotation matrix, trigonometric relationships are used, such as the functions atan2, sin, and cos. The results of these calculations provide unique values for each angle, with certain constraints to ensure that the results are consistent and unambiguous.

### 2.2.1 Euler and Quaternion Angle

Euler angles are often used to represent rotation in three-dimensional space with three angles, namely yaw, pitch, and roll. However, this approach has several drawbacks that make it less than ideal for many applications, especially those related to robotic simulation and control or dynamics. One of the main drawbacks of Euler angles is gimbal lock, which is a situation where two of the three rotation axes are parallel to each other. When this happens, the system loses one degree of freedom, making it difficult to represent rotation correctly.

Gimbal lock makes rotation ambiguous and cannot be represented uniquely, which causes errors in data processing. This is a major problem in systems that require high accuracy, such as flight control, motion simulation, or orientation-dependent robot manipulation.

In addition to gimbal lock, Euler angles also have problems related to rotation interpolation, which is difficult to do smoothly(Li & Wang, 2013). When wanting to make continuous rotation changes, Euler angles often show unwanted changes or jump between angles, which causes simulations or calculations to become unstable. Below is the Euler equation at Eq. 2-6 – Eq.2-8 to find the angle roll (θ)(θ), pitch (φ)(φ), yaw (ψ(ψ).

$$Rz(\psi) = \begin{pmatrix} \cos(\psi) & -\sin(\psi) & 0 \\ \sin(\psi) & \cos(\theta) & 0 \\ 0 & 0 & 1 \end{pmatrix} \quad (2-6)$$

$$Rx(\theta) = \begin{pmatrix} 1 & 0 & 0 \\ 0 & \cos(\theta) & -\sin(\theta) \\ 0 & \sin(\theta) & \cos(\theta) \end{pmatrix} \quad (2-7)$$

$$Ry(\varphi) = \begin{pmatrix} \cos(\varphi) & 0 & \sin(\varphi) \\ 0 & 1 & 0 \\ -\sin(\varphi) & 0 & \cos(\varphi) \end{pmatrix} \quad (2-8)$$

$$Mrot = \begin{pmatrix} r11 & r12 & r13 \\ r21 & r22 & r23 \\ r31 & r32 & r33 \end{pmatrix} \quad (2-9)$$

$$\psi = arctan2(r21, r11) \quad (2-10)$$

$$\theta = arcsin(-r31) \quad (2-11)$$

$$\varphi = arctan2(r32, r33) \quad (2-12)$$

Calculating Euler angles with IMU data it can solve with equation Eq. 2-13 – Eq. 2-14:

$$Pitch\ (\theta) = \arctan\left(\frac{-ax}{\sqrt{ay^2 + az^2)}}\right) \quad (2-13)$$

$$Roll\ (\varphi) = \arctan\left(\frac{ay}{\sqrt{ay^2 + az^2)}}\right) \quad (2-14)$$

To overcome value distortion when rotating on the x and y axes, compensation needs to be carried out with the compensation Magnetometer Eq. 2-17.

Tilt Compensation (Roll and Pitch):

(Magnetometer mx, my, mz)

$$mx' = mx\cos(\theta) + mz\sin(\theta) \quad (2-15)$$

$$my' = mx\sin(\varphi)\sin(\theta) + my\cos(\varphi) - mz\sin(\varphi)\cos(\theta) \quad (2-16)$$

$$\psi = arctan2(-my', mx') \quad (2-17)$$

To provide dynamic movement corrections at all times, Eq. 2-18 – 2-20, it is necessary to make corrections using the gyroscope axis.

Angle correction with Gyroscope:

(Gyroscope gx,gy,gz)

$$\varphi = \varphi t - 1 + gx.\Delta T \quad (2-18)$$

$$\theta = \theta t - 1 + gy.\Delta T \quad (2-19)$$

$$\psi = \psi t - 1 + gz.\Delta T \quad (2-20)$$

Therefore, to overcome these drawbacks, quaternions are often used as an alternative. Quaternion is able to represent rotation in three-dimensional space without experiencing gimbal lock and has smoother and more stable interpolation capabilities(Youn & Andrew Gadsden, 2019). With a quaternion, rotation can be implemented more accurately, free from the constraints experienced by the Euler angles. Below is the quaternion equation Eq. 2-21 to overcome the value distortion.

Equation Quaternion:

$$\begin{aligned} Qw &= \cos\left(\frac{\varphi}{2}\right)\cos\left(\frac{\theta}{2}\right)\cos\left(\frac{\psi}{2}\right) + \sin\left(\frac{\varphi}{2}\right)\sin\left(\frac{\theta}{2}\right)\sin\left(\frac{\psi}{2}\right) \\ Qx &= \sin\left(\frac{\varphi}{2}\right)\cos\left(\frac{\theta}{2}\right)\cos\left(\frac{\psi}{2}\right) - \cos\left(\frac{\varphi}{2}\right)\sin\left(\frac{\theta}{2}\right)\sin\left(\frac{\psi}{2}\right) \\ Qy &= \cos\left(\frac{\varphi}{2}\right)\sin\left(\frac{\theta}{2}\right)\cos\left(\frac{\psi}{2}\right) + \sin\left(\frac{\varphi}{2}\right)\cos\left(\frac{\theta}{2}\right)\sin\left(\frac{\psi}{2}\right) \\ Qz &= \cos\left(\frac{\varphi}{2}\right)\cos\left(\frac{\theta}{2}\right)\sin\left(\frac{\psi}{2}\right) - \sin\left(\frac{\varphi}{2}\right)\sin\left(\frac{\theta}{2}\right)\cos\left(\frac{\psi}{2}\right) \end{aligned} \quad (2-21)$$

Return the equation to Euler from Eq. 2-22 – Eq. 2-24:

$$Yaw\ (\psi) = arctan2\big(2(QwQz + QxQy), 1 - 2(Qy^2 + Qz^2)\big) \quad (2-22)$$

$$Pitch\ (\theta) = arcsin\big(2(QwQy - QzQx)\big) \quad (2-23)$$

$$Roll\ (\varphi) = arctan2\big(2(QwQx + QyQz), 1 - 2(Qx^2 + Qy^2)\big) \quad (2-24)$$

### 2.3. Kalman Filter Implementation

The Kalman Filter is a mathematical algorithm designed to estimate the state of a dynamic system, even though the measurements of the system are noisy. The Kalman Filter works by combining predictions based on a system model with actual measurement data to provide the best estimate of the state of the system (Wicaksono et al., 2020). This estimation is done iteratively over time, making it very useful in various real-time applications. The following are two stages in the Kalman filter, namely the prediction stage on Eq. 2-25 and the update stage on Eq. 2-28.

Prediction Stage :

$$\hat{x}_{k|k-1} = A\hat{x}_{k-1|k-1} + Bu_k \quad (2-25)$$

Prediction Covariance Error:

$$P_{k|k-1} = AP_{k-1|k-1}A^T + Q \quad (2-26)$$

Kalman Gain:

$$K_k = P_{k|k-1}H^T(HP_{k|k-1}H^T + R)^{-1} \quad (2-27)$$

Update Stage:

$$\hat{x}_{k|k} = \hat{x}_{k|k-1} + K_k(z_k - H\hat{x}_{k|k-1}) \quad (2-28)$$

Update Covariance Error:

$$P_{k|k} = (I - K_kH)P_{k|k-1} \quad (2-30)$$

After we know the equation of the Kalman filter, we can filter the data from the Euler angles for each, such as the roll, pitch, and yaw angles. Then the following equation Eq. 2-31 can be obtained.

Rotation Matrix:

$$R = \begin{pmatrix} \cos(\psi)\cos(\theta) & \cos(\psi)\sin(\theta)\sin(\varphi) - \sin(\psi)\cos(\varphi) & \cos(\psi)\sin(\theta)\cos(\varphi) + \sin(\psi)\sin(\varphi) \\ \sin(\psi)\cos(\theta) & \sin(\psi)\sin(\varphi) + \cos(\psi)\cos(\varphi) & \sin(\psi)\sin(\theta)\cos(\varphi) - \cos(\psi)\sin(\varphi) \\ -\sin(\theta) & \cos(\theta)\sin(\varphi) & \cos(\theta)\cos(\varphi) \end{pmatrix} \quad (2-31)$$

## 2.4 Ground Control Station (GCS)

Ground Control Station is able to receive data provided by the Cansat vehicle in real time (Abdul Razak et al., 2020). In a satellite launch mission, information is needed about all data obtained by the satellite in real time. A system is also needed to display all information that has been received; this requires software that is able to process all information. So a ground control station was created as a container for information that has been obtained and then visualized directly, so that it can be directly monitored by humans on Earth.

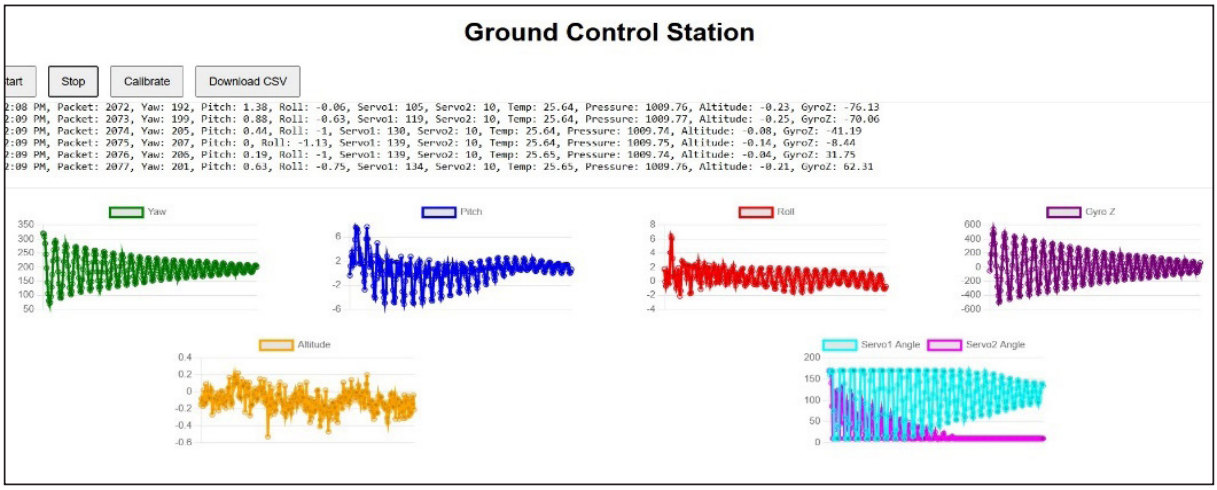


**Figure 2-6:** User Interface of GCS.

GCS receives data from the CanSat vehicle with wi-fi telemetry using the WebSocket protocol. For data sending, the sampling time is 20 ms. With one data packet sending consisting of " Time, Packet Count, Yaw, Pitch, Roll, Angle SV1, Angle SV2, Temperature, Air Pressure, Altitude, GyroZ, " it can show the (Figure 2-6), which is a chart of the data received by GCS.

then all the data is exported in CSV format for further analysis. For plot display, it can be seen in real-time, such as angle, altitude, angular, and velocity.

## 3. Result and Analysis

### 3.1 Accelerometer Data Filter

Basically, the accelerometer sensor is used to measure the acceleration of an object, then determine its direction. But in reality, there is often noise on each axis. To overcome this, it is necessary to use a filter such as a moving average, which the author uses to handle bias and noise on the accelerometer sensor, for example, in (Figure 3-1) and (Figure 3-3).

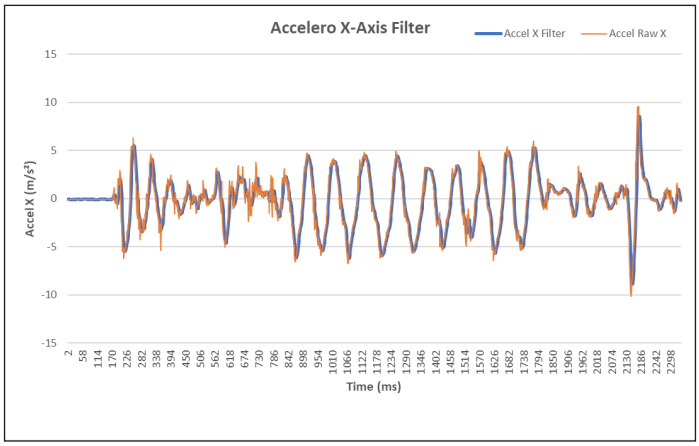


**Figure 3-1:** Chart of Accelerometer X axes.

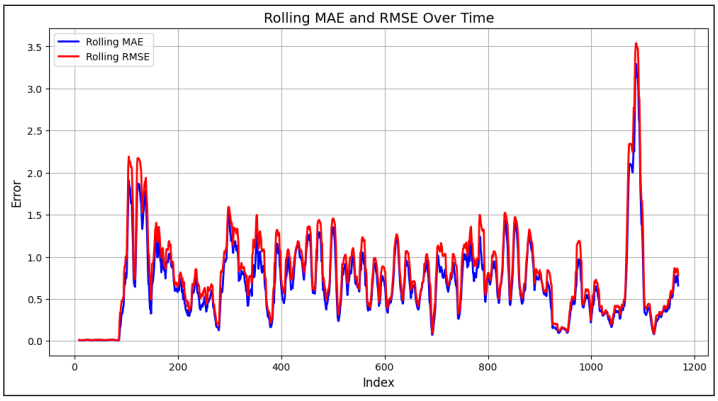


**Figure 3-2:** Accelerometer X Filter Accuracy and Stability.

With the filter results using moving average showing the accuracy and stability of the accelerometer x axes with data in Table 3-1, the results are MAE and RMSE based on raw data and after filtering on accelerometer x axes (Figure 3-2).

**Table 3-1**: Data Result based on Noise and Filter Accelerometer X Axes

| Mean Absolute Error (MAE) | Root Mean Square Error (RMSE) | Stability Filter | Accuracy Filter |
|---|---|---|---|
| 0.68 | 16.09 | 8.08 % | 28.08 % |

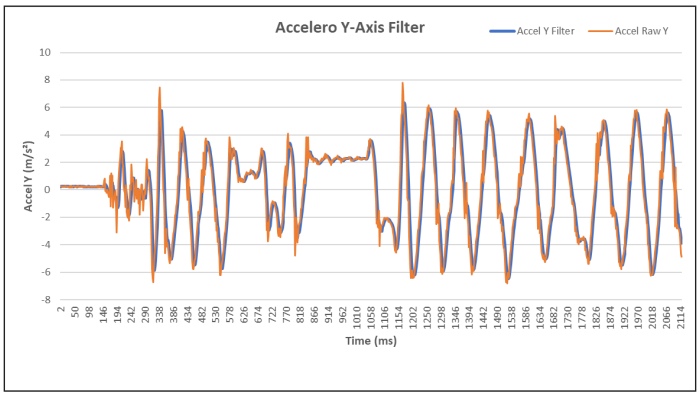


**Figure 3-3:** Chart of Aceelerometer Y axes.

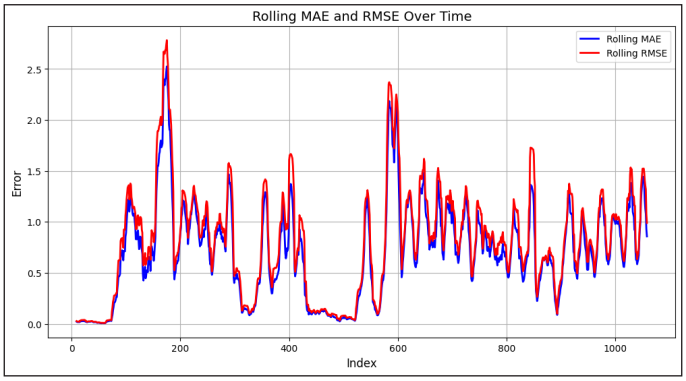


**Figure 3-4:** Accelerometer Y Filter Accuracy and Stability.

With the filter results using moving average showing the accuracy and stability of the accelerometer y axes with data in Table 3-2, the results are MAE and RMSE based on raw data and after filtering on accelerometer y axes (Figure 3-4).

**Table 3-2:** Data Result based on Noise and Filter Accelerometer Y Axes

| Mean Absolute Error (MAE) | Root Mean Square Error (RMSE) | Stability Filter | Accuracy Filter |
|---|---|---|---|
| 0.711 | 0.970 | 6.29 % | 26.66 % |

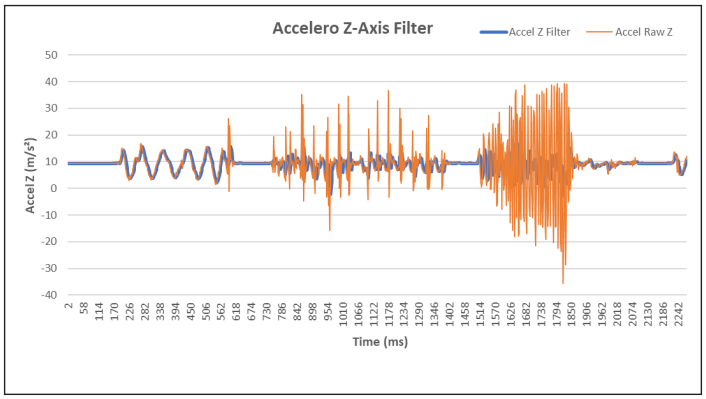


**Figure 3-5:** Chart of Accelerometer Z axes.

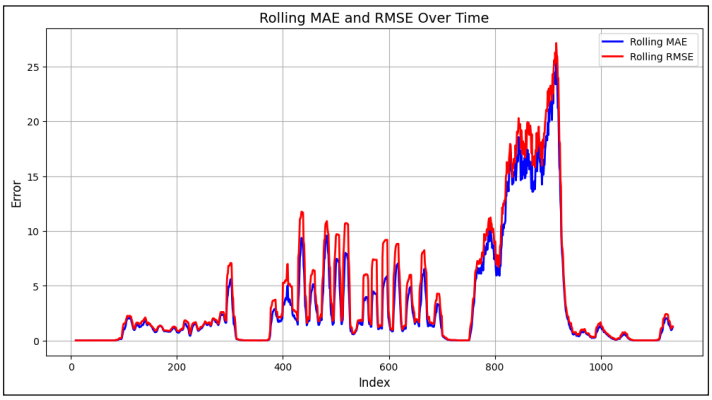


**Figure 3-6:** Accelerometer Z Filter Accuracy and Stability.

With the filter results using moving average showing the accuracy and stability of the accelerometer z axes with data in Table 3-3, the results are MAE and RMSE based on raw data and after filtering on accelerometer z axes (Figure 3-6).

**Table 3-3:** Data Result based on Noise and Filter Accelerometer Z Axes

| Mean Absolute Error (MAE) | Root Mean Square Error (RMSE) | Stability Filter | Accuracy Filter |
|---|---|---|---|
| 3.38 | 6.98 | 89.38 % | 51.54 % |

Based on the case of the accelerometer sensor, the moving average filter has a significant impact on the filter result, able to reduce noise in dynamic conditions with satisfactory consistency. Moving average here uses a filter size (*t-5*) to estimate the error value of the result. This gives a good result with a short process.

### 3.2 Gyroscope Data Filter

Gyroscope sensors are used to measure the angular velocity of an object. But in reality, noise often occurs on each axis, both in static and dynamic conditions. To overcome this, a filter is needed, such as a moving average, that the author uses to handle bias and noise on the gyroscope sensor, for example, on (Figure 3-7) and (Figure 3-9).

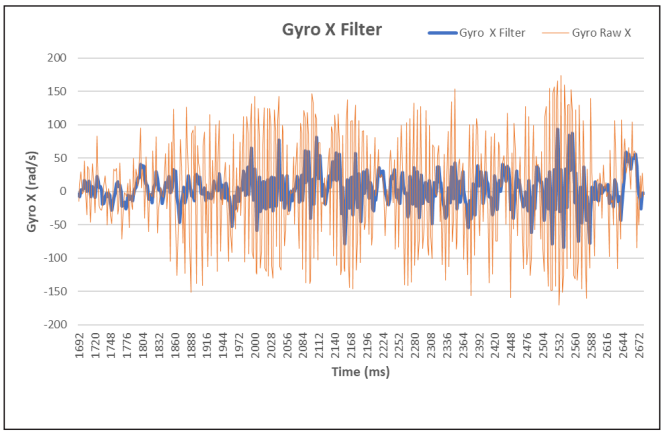


**Figure 3-7:** Chart of Gyroscope X axes.

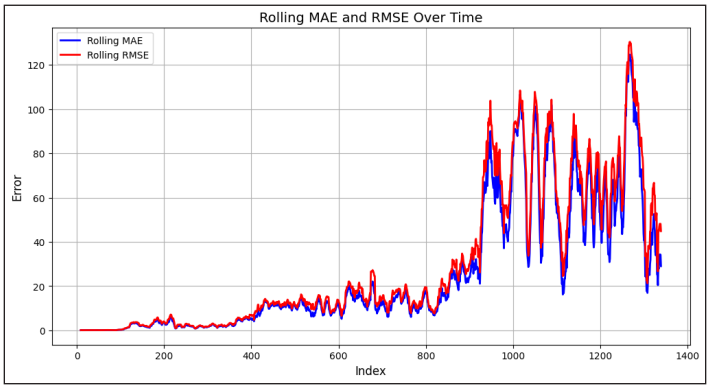


**Figure 3-8:** Gyro X Filter Accuracy and Stability.

With the filter results using moving average showing the accuracy and stability of the gyroscope x axes with data in Table 3-4, the results are MAE and RMSE based on raw data and after filtering on the gyroscope x axes (Figure 3-8).

**Table 3-4:** Data Result based on Noise and Filter Gyro X Axes

| Mean Absolute Error (MAE) | Root Mean Square Error (RMSE) | Stability Filter | Accuracy Filter |
|---|---|---|---|
| 25.47 | 43.62 | 89.78 % | 41.60 % |

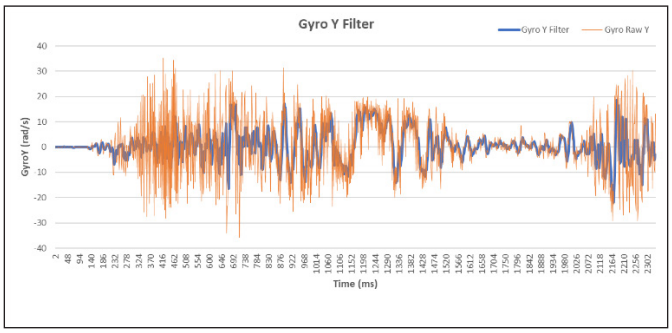


**Figure 3-9:** Chart of Gyroscope Y axes.

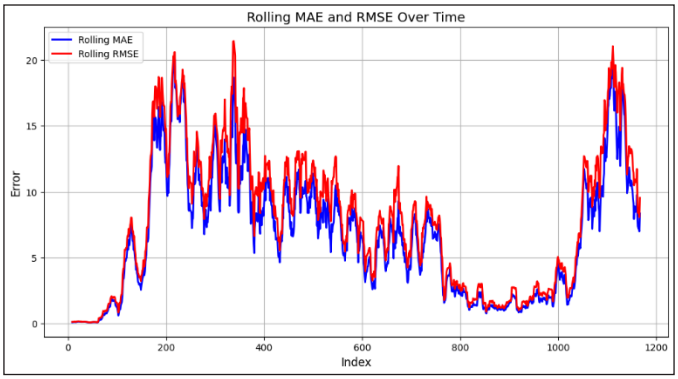


**Figure 3-10:** Gyro Y Filter Accuracy and Stability

With the filter results using moving average showing the accuracy and stability of the gyroscope y axes with data in Table 3-5, the results are MAE and RMSE based on raw data and after filtering on the gyroscope y axes (Figure 3-10).

**Table 3-5:** Data Result based on Noise and Filter Gyro Y Axes

| Mean Absolute Error (MAE) | Root Mean Square Error (RMSE) | Stability Filter | Accuracy Filter |
|---|---|---|---|
| 6.70 | 9.62 | 72.69 % | 29.55 % |

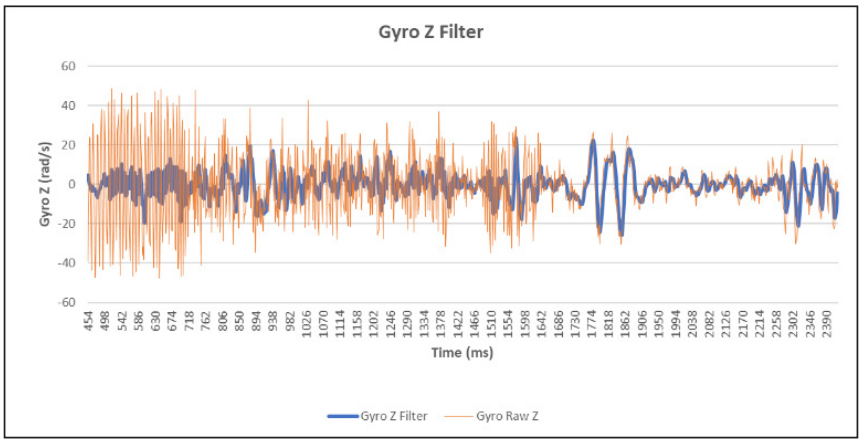


**Figure 3-11:** Chart of Gyroscope Z axes.

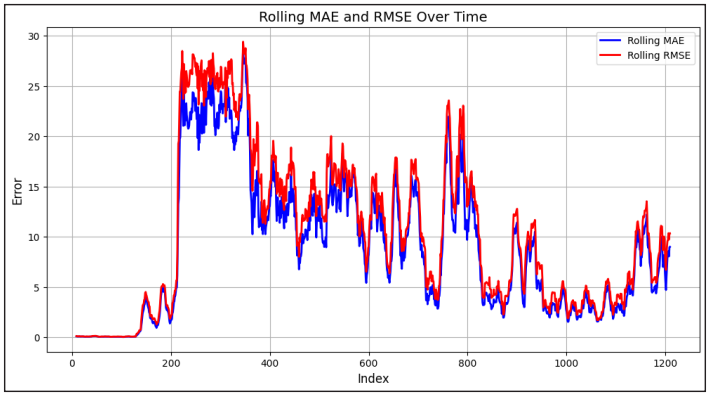


**Figure 3-12:** Gyro Z Filter Accuracy and Stability.

With the filter results using moving average showing the accuracy and stability of the gyroscope z axes with data in Table 3-6, the results are MAE and RMSE based on raw data and after filtering on the gyroscope z axes (Figure 3-12).

**Table 3-6:** Data Result based on Noise and Filter Gyro Z Axes

| Mean Absolute Error (MAE) | Root Mean Square Error (RMSE) | Stability Filter | Accuracy Filter |
|---|---|---|---|
| 8.99 | 13.13 | 79.09 % | 31.49 % |

Based on the case of the gyroscope sensor, the moving average filter has a significant impact on the filter result, able to reduce noise in dynamic and static conditions with satisfactory consistency. Moving average here uses filter size (t-5) to estimate the error value of the result after. This gives a good result with a short process.

### 3.3 Roll Angle Kalman filter

Testing on the roll angle is done by comparing the roll value before using the Kalman filter and after using the Kalman filter with dynamic and static conditions, as seen in (Figure 3-13). When the static graph is at a value with a certain time interval, it means that the IMU condition is in a still or static condition. And it can also be seen that when the IMU value moves towards a value of 90 degrees, the graph will move up the vertical axis, and if the value goes to -90, the graph will go down the vertical axis.

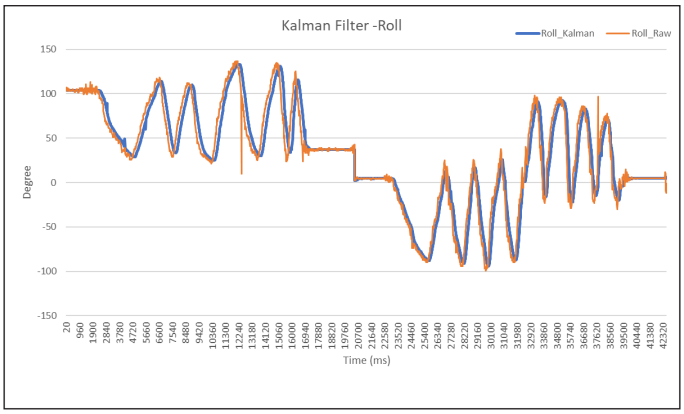


**Figure 3-13:** Chart Angle Roll with Kalman Filter.

From the test results of the graph above, the values of Q = 0.02, R = 0.01, P = 0.01 are given, it can be analyzed that the Kalman response provides smoother results when the conditions are static and dynamic, it can be compared to the response at the roll angle before being filtered which tends to be noisy when the conditions are static, and there is fluctuation when the conditions are dynamic, this proves that the Kalman filter provides good and accurate response results.

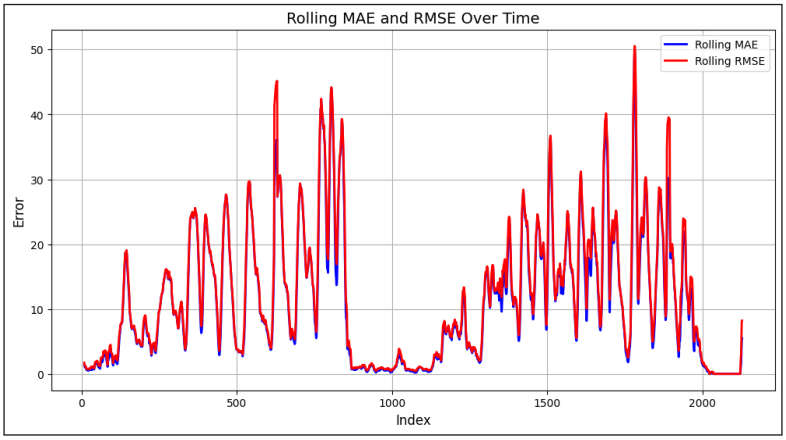


**Figure 3-14:** Roll Angle Accuracy and Stability with RMSE and MAE.

**Table 3-7:** Data Result based on Noise and Filter Roll Angle

| Mean Absolute Error (MAE) | Root Mean Square Error (RMSE) | Stability Filter | Accuracy Filter |
|---|---|---|---|
| 11.33 | 15.96 | 1.71 % | 28.99 % |

A t-test was conducted to assess the statistical significance of improvements observed in angular stability post-filtering. The results indicated a p-value < 0.05, confirming that the observed improvements were statistically significant. However, the Kalman Filter's performance may degrade in the presence of sudden sensor anomalies, suggesting the need for adaptive tuning or hybrid filtering approaches.

From the data in Table 3-7. We get some data that we can analyze, such as MAE, which shows a value of 11.33, which is a fairly low average error, which means that the previous raw data results were less accurate, and then, after going through the Kalman filter, gave better results. RMSE 15.96 is higher than MAE, indicating that some outliers or deviations are greater than the raw data at some points.

With this, the Kalman filter at the roll angle increased stability of 1.71% which shows more stable results than the raw data. Then, for accuracy, the difference in RMSE and MAE was measured at 28.99% which means providing improved filter performance from improvements to incoming raw data.

### 3.4 Pitch Angle Kalman filter

Testing on the pitch angle is done by comparing the pitch value before using the Kalman filter and after using the Kalman filter with dynamic and static conditions, as seen in (Figure 3-15). When the static graph is at a value with a certain time interval, it means that the IMU condition is in a still or static condition. And it can also be seen that when the IMU value moves towards a value of 90 degrees, the graph will move up the vertical axis, and if the value goes to -90, the graph will go down the vertical axis.

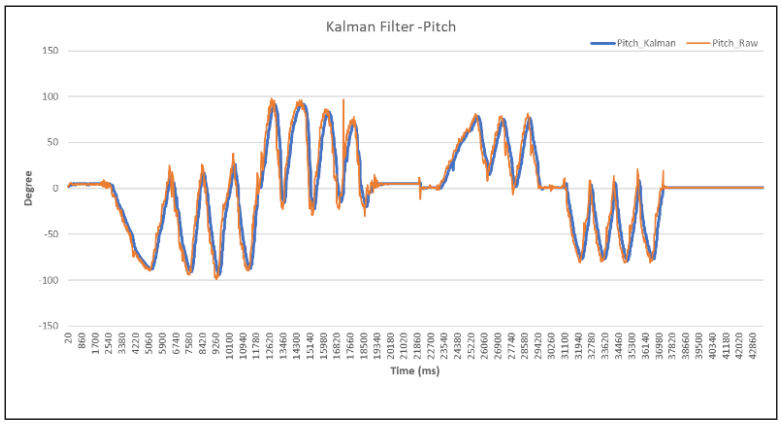


**Figure 3-15:** Chart Angle Pitch with Kalman Filter.

From the test results of the graph above, the values of Q = 0.02, R = 0.01, P = 0.01 are given, it can be analyzed that the Kalman response provides smoother results when the conditions are static and dynamic, it can be compared to the response at the pitch angle before being filtered which tends to be noisy when the conditions are static, and there is

fluctuation when the conditions are dynamic, this proves that the Kalman filter provides good and accurate response results.

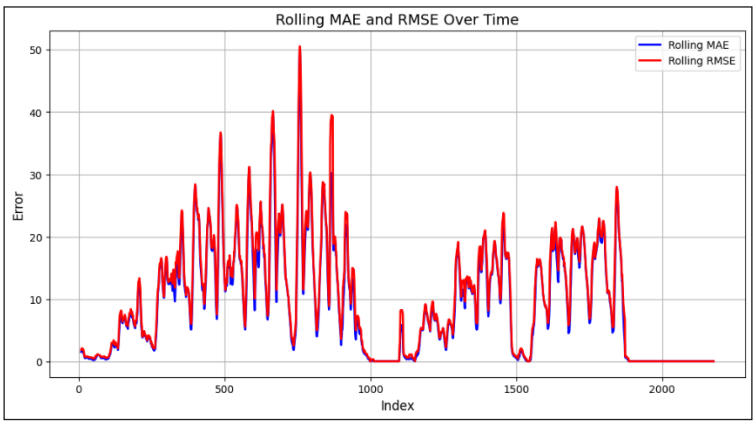


**Figure 3-16:** Pitch Angle Accuracy and Stability with RMSE and MAE.

**Table 3-8:** Data Result based on Noise and Filter Pitch Angle

| Mean Absolute Error (MAE) | Root Mean Square Error (RMSE) | Stability Filter | Accuracy Filter |
|---|---|---|---|
| 9.47 | 13.75 | 4.63 % | 31.12 % |

From the data in Table 3-8, we get some data that we can analyze, such as MAE, which shows a value of 9.47, which is a fairly low average error, which means that the previous raw data results were less accurate, and then, after going through the Kalman filter, gave better results. RMSE 13.75 is higher than MAE, indicating some outliers or deviations are greater than the raw data at some points.

With this, the Kalman filter at the pitch angle increased stability of 4.63% which shows more stable results than the raw data. Then, for accuracy, the difference in RMSE and MAE was measured at 31.12% which means providing improved filter performance from improvements to incoming raw data.

### 3.5 Yaw Angle Kalman filter

Testing on the yaw angle is done by comparing the yaw value before using the Kalman filter and after using the Kalman filter with dynamic and static conditions, as seen in (Figure 3-17). when the static graph is at a value with a certain time interval, it means that the IMU condition is in a still or static condition. And it can also be seen when the IMU value moves towards a value of 180 degrees, the graph will move up the vertical axis, and if the value goes to 90, the graph will go down the vertical axis.

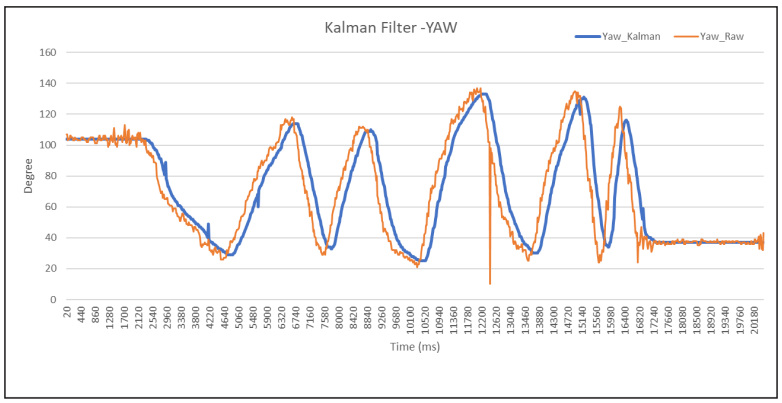


**Figure 3-17:** Chart Angle Yaw with Kalman Filter.

From the test results of the graph above, the values of Q = 0.05, R = 0.01, P = 0.03 are given, it can be analyzed that the Kalman response provides smoother results when the conditions are static and dynamic, it can be compared to the response at the yaw angle before being filtered, which tends to be noisy when the conditions are static, and there is fluctuation when the conditions are dynamic, this proves that the Kalman filter provides good and accurate response results.

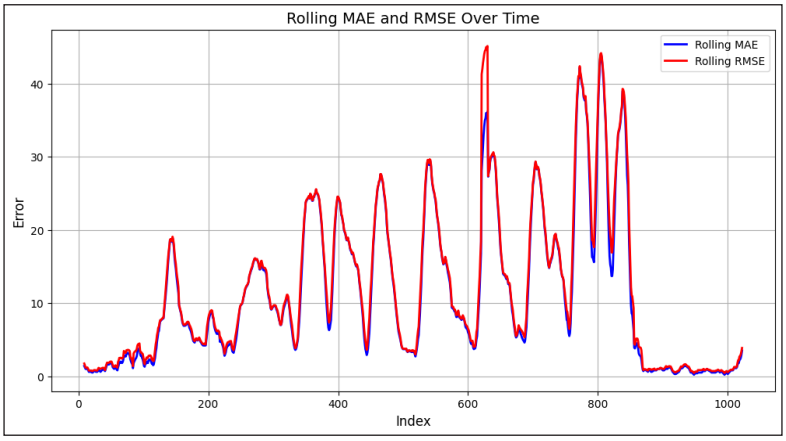


**Figure 3-18:** Pitch Angle Accuracy and Stability with RMSE and MAE.

**Table 3-9:** Data Result based on Noise and Filter Yaw Angle

| Mean Absolute Error (MAE) | Root Mean Square Error (RMSE) | Stability Filter | Accuracy Filter |
|---|---|---|---|
| 11.38 | 16.06 | 5.29 % | 29.25 % |

From the data in Table 3-9. we get some data that we can analyze, such as MAE, which shows a value of 11.38, which is a fairly low average error, which means that the previous raw data results were less accurate, then after going through the Kalman filter gave better results. RMSE 16.09 is higher than MAE, indicating that some outliers or deviations are greater than the raw data at some points.

With this, the Kalman filter at the yaw angle increased stability of 5.29% which shows more stable results than the raw data. Then, for accuracy, the difference in RMSE and MAE was

measured at 29.25% which means providing improved filter performance from improvements to incoming raw data.

### 3.6 Angle of Camera Pointing

To obtain a certain direction of facing, it is necessary to use the configuration of each joint on the parallel manipulator. Therefore, the use of inverse kinematics is very helpful to configure each joint, so that the given angle reference can be directly calculated to the desired direction of facing. Below can be seen in (Figure 3-19) how forward kinematics plays a role in adjusting each joint angle from the given IMU reference; the YAW heading reference can be seen in (Figure 3-20).

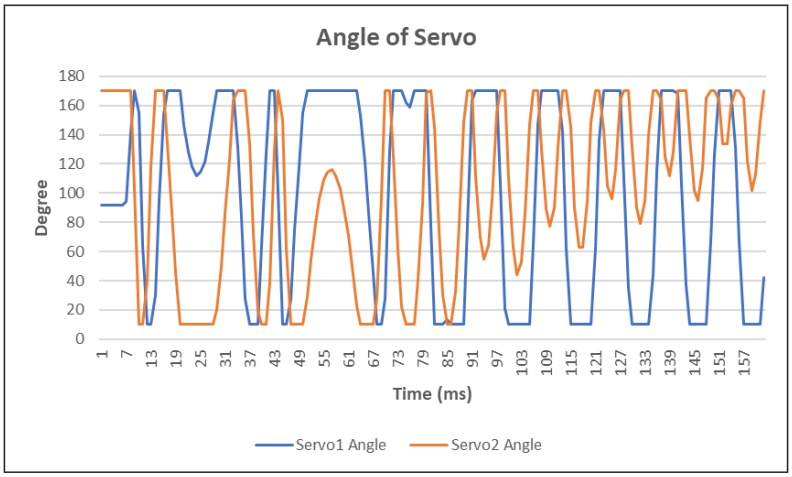


**Figure 3-19:** Angle Servo for each joint.

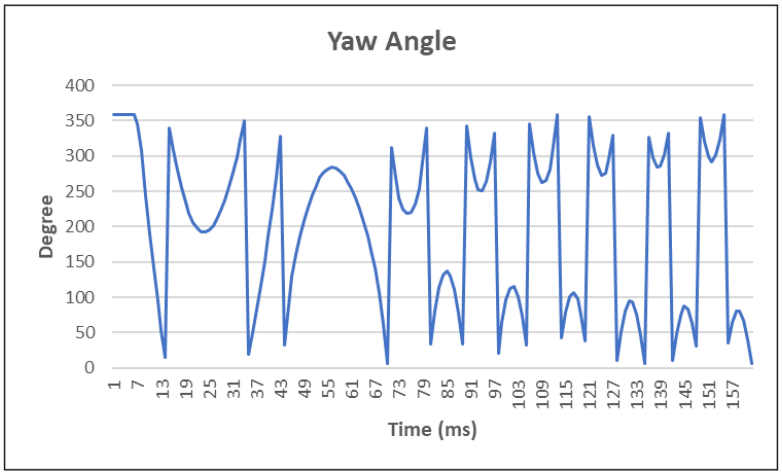


**Figure 3-20:** Reference Angle to Pointing Camera.

From the results above, it can be seen that each reference change gives the value of each parallel manipulator joint, still maintaining the same direction. but here it is necessary to pay attention to the impact of the singularity of the design used, so that the joint must only be able to move with a range of angle values of 10 degrees to 170 degrees to maintain its absolute position.

### 3.7 Camera Result

The output of this research is used to face a camera at a 45-degree angle and in one direction. (Figure 3-21) shows the position of the camera angle and several variations in the direction of the face, which represents when the vehicle is flying, it is able to direct the camera to a certain point to maintain the stability of the video recording.

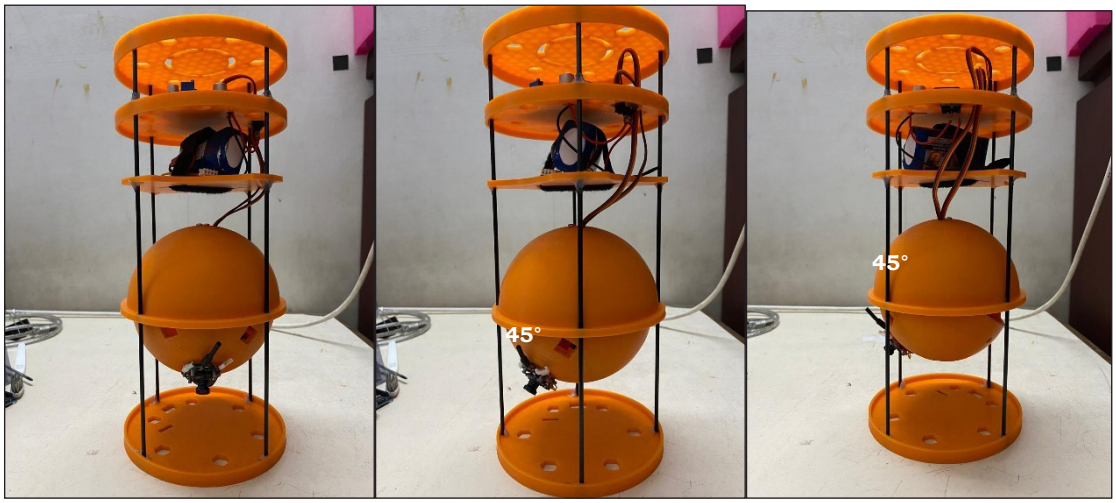


**Figure 3-21:** Parallel Manipulator Pointing 45° Camera.

The author has also conducted a test when the vehicle is facing west, and when the CanSat rotates 360 degrees, the parallel manipulator can keep the camera facing direction stable in the west direction as seen in (Figure 3-22). shows the camera remains in the same direction thanks to the help of the parallel manipulator. With this, the CAN Satellite can survive in various conditions and orientations, so that video recordings during flight can be analyzed more easily and help further research.

**Figure 3-22:** Camera Capture Pointing West Direction

## 4. Conclusions

This research proves that the application of the Kalman filter as a filtering method for estimating roll, pitch, and yaw angles on a parallel manipulator system has a significant positive impact on system performance. The results obtained show that the Kalman filter effectively filters noise in raw sensor data, resulting in smoother and more stable estimated angles. Yaw stability improved by 5.29% with 29.25% better filter accuracy, pitch stability increased by 4.63% with 31.12% filter accuracy improvement, and roll stability was enhanced by 1.71%

with 28.99% better filter accuracy. This filtering process provides an important increase in accuracy in manipulator control, especially in handling unstable sensor data collisions.

In the applications on CAN satellites, parallel manipulators controlled based on this filtered data demonstrate a strong ability to maintain camera orientation toward the desired target. The manipulator consistently maintains the camera's direction, even when the satellite experiences various orientation variations due to external motion or disturbances. This shows that the system can adapt dynamically to environmental changes without losing precision control.

The Kalman Filter demonstrated superior performance in maintaining angular stability compared to the Moving Average Filter, particularly under dynamic conditions. Future research could explore the implementation of the Extended Kalman Filter (EKF) or the Unscented Kalman Filter (UKF) to address non-linearities in sensor data. Additionally, the insights from this study could be extended to broader satellite applications, including remote sensing and atmospheric data collection.

This improvement in camera orientation stability significantly impacts practical applications, such as video recording, resulting in more stable recordings with better image quality due to minimal oscillation effects or disturbances. Thus, this study makes a significant contribution to the development of IMU data-based manipulator control technology for small satellite applications and similar systems requiring high orientation stability. The results of this study open opportunities for further development in Kalman filter parameter optimization and integration with more sophisticated control algorithms to support more complex applications in the future.

This research paves the way for further exploration into adaptive Kalman Filter models and hybrid control algorithms. Future work could focus on incorporating neural networks to enhance Kalman Filter adaptability and extend testing to more diverse operational environments, such as varying altitudes and rotational speeds.

## Acknowledgements

The author extends sincere gratitude to the colleagues and peers of the Bamantara Eepisat team for their invaluable support and contributions throughout this research. Special appreciation is also directed to the advisor for consistently providing insightful guidance and solutions to the author.

## Contributorship Statement

This research aims to contribute to the development of Can Satellite technology in preparation for participation in the United States CanSat 2025 competition.

## References

Abdul Razak, N. T., Majid, H. A., Saparuddin, F. A., Abdul Jalil, M. F., Jamaluddin Jalil, M. S., & Mokhtar, M. H. (2020). The Ground Control Station Design For Can-Sized Satellite (CanSAT) System. *International Journal of Advanced Technology in Mechanical, Mechatronics and Materials*, *1*(2), 76–82. https://doi.org/10.37869/ijatec.v1i2.24

Asundi, S. A., & Fitz-Coy, N. G. (2013). Design of command, data and telemetry handling system for a distributed computing architecture CubeSat. *IEEE Aerospace Conference Proceedings*. https://doi.org/10.1109/AERO.2013.6496901

Fadaei, M. H. K., Zalaghi, A., Atigh, S. G. R. A. G., & Torkani, Z. (2019). Design of PID and Fuzzy-PID Controllers for Agile Eye Spherical Parallel Manipulator. *2019 IEEE 5th Conference on Knowledge Based Engineering and Innovation : February 28th & March 1st, Iran*

*University of Science and Technology, Tehran, Iran*. IEEE. https://doi.org/10.1109/KBEI.2019.8735095

Farahan, S. B., Machado, J. J. M., de Almeida, F. G., & Tavares, J. M. R. S. (2022). 9-DOF IMU-Based Attitude and Heading Estimation Using an Extended Kalman Filter with Bias Consideration. *Sensors*, *22*(9). https://doi.org/10.3390/s22093416

Kadir, R. E. A., Sahal, M., Jagad, G., Jazidie, A., & Hidayat, Z. (2020). Application of Kalman Filter in Fine Alignment of INS Assisted by Magneto Sensors. *Proceedings, 2020 International Seminar on Intelligent Technology and Its Application (ISITIA 2020) : Humanification of reliable intelligent systems : 22-23 July 2020, virtual conference*. IEEE. https://doi.org/10.1109/ISITIA49792.2020.9163763

Li, W., & Wang, J. (2013). Effective adaptive kalman filter for MEMS-IMU/magnetometers integrated attitude and heading reference systems. *Journal of Navigation*, *66*(1), 99–113. https://doi.org/10.1017/S0373463312000331

Narasimhappa, M., Mahindrakar, A. D., Guizilini, V. C., Terra, M. H., & Sabat, S. L. (2020). MEMS-Based IMU Drift Minimization: Sage Husa Adaptive Robust Kalman Filtering. *IEEE Sensors Journal*, *20*(1), 250–260. https://doi.org/10.1109/JSEN.2019.2941273

Palmieri, G., Callegari, M., Carbonari, L., & Palpacelli, M. C. (2014). Design and testing of a spherical parallel mini manipulator. *Mechatronic and Embedded Systems and Applications (MESA) 2014 - IEEE/ASME 10th International Conference on Mechatronic and Embedded System and Applications*. https://doi.org/10.1109/mesa.2014.6935523

Ramadhan, R. P., Ramadhan, A. R., Putri, S. A., Latukolan, M. I. C., Edwar, & Kusmadi. (2019). Prototype of CanSat with Auto-gyro Payload for Small Satellite Education. *2019 IEEE 13th International Conference on Telecommunication Systems, Services, and Applications (TSSA). Pp. 243-248.* https://doi.org/10.1109/TSSA48701.2019.8985514

Urandra, A. E., Dirgantoro, B., & Syihabuddin, B. (2016). Design of On Board Data Handling using raspberry pi for nanosatellite payload. *International Conference on Control, Electronics, Renewable Energy, and Communications (ICCEREC)*, pp. 110-114. https://doi.org/10.1109/ICCEREC.2016.7814954

Wicaksono, M. A. R., Kurniawan, F., & Lasmadi, L. (2020). Kalman Filter untuk Mengurangi Derau Sensor Accelerometer pada IMU Guna Estimasi Jarak. *AVITEC*, *2*(2). https://doi.org/10.28989/avitec.v2i2.752

Youn, W., & Andrew Gadsden, S. (2019). Combined quaternion-based error state kalman filtering and smooth variable structure filtering for robust attitude estimation. *IEEE Access*, *7*, 148989–149004. https://doi.org/10.1109/ACCESS.2019.2946609